Angular moments models for rarefied gas dynamics. Numerical comparisons with kinetic and Navier-Stokes equations.

Sbastien Guisset[1]

Abstract. Angular moments models based on a minimum entropy problem have been largely used to describe the transport of photons [15] or charged particles [20]. In this communication the M_1 and M_2 angular moments models are presented for rarefied gas dynamics applications. After introducing the models studied, numerical simulations carried out in various collisional regimes are presented and illustrate the interest in considering angular moments models for rarefied gas dynamics applications. For each numerical test cases, the differences observed between the angular moments models and the well-known Navier-Stokes equations are discussed and compared with reference kinetic solutions.

Key words: Angular moments models, minimum entropy closure, rarefied gas dynamics, Navier-Stokes equations, kinetic equations.

1 Introduction

While kinetic descriptions can be considered to describe accurately the transport of particles in rarefied gas dynamics [16] they are also known to be computationally expensive. In order to keep relatively low computational cost, a possible solution consists in working with reduced descriptions which describe the temporal evolution of macroscopic physical quantities. Unfortunately, standard velocity moments models are often not satisfactory since they can be particularly inaccurate. Indeed the particles studied may have a probability distribution function far from the Maxwellian equilibrium distribution so that traditional reduced descriptions become useless. One understands here the difficulty in capturing kinetic effects using reduced kinetic codes operating on fluid time scales [14, 23].

Angular moments models represent alternative methods between the kinetic and the macroscopic models (velocity moments models). Indeed, they require computational times shorter than kinetic models and provide results

[1]CEA, DAM, DIF, F-91297 Arpajon, France. E-mail: sebastien.guisset@cea.fr

with a higher accuracy than most of standard fluid models. While velocity moments models are obtained by integrating in velocity the kinetic equations (against weight functions), angular moments models only consider an angular integration (integration on the unit sphere). Basically, the main idea is to keep the velocity modulus (denoted ζ in this work) as a (kinetic) variable (such as space and time). This simple idea leads to the derivation of an hierarchy of angular moments equations and set the angular moments models as natural candidates to study far equilibrium regimes at a relatively low numerical cost.

Similarly to velocity moments models, angular moments models requires a closure relation. Over the years various closures have been investigated. In this document, angular moments models based on a minimum entropy problem are considered [9]. This kind of closure have been widely studied in [34, 27, 32, 33, 38, 1, 29, 41, 30]. The resolution of this closure problem leads to consider an underlying distribution function under the form of an exponential of a polynomial (of the weight functions considered). Therefore this underlying distribution function is non negative. Such a closure relation also gives fundamental mathematical properties [27, 37, 25] to the resulting moments models such as hyperbolicity and entropy dissipation. However, their solutions could be rather different from the solution of the kinetic equation.

The idea to perform an angular integration has been largely used in the context of radiative transfer [43, 2, 10, 42, 7, 35, 36] and is currently extending to other fields, such as plasma physics [9, 20, 21, 19] or radiotherapy applications [12, 40]. Here, the dynamics of neutral particles in dilute gas is investigated.

The present study is original for two main reasons. First of all, very few works considers the use of angular moments models (not velocity moments models) based on a minimum entropy closure applied to rarefied gas dynamics. To our knowledge there is only the work proposed in [18] and the differences with the present communication will be explained. Secondly, clear numerical comparisons with Navier-Stokes and reference kinetic solutions are presented in various collisional regimes. This study is different with all the works involving a minimum entropy closure since only an angular integration is performed. In addition, the work proposed in [18] is a first step towards the modeling and simulation involving two distinct species of particle (heavy and light particles for example). This explain why a framework centered on the particles mean velocity was considered. Unfortunately, this choice brings many difficulties at the discrete level to enforce the zero mean velocity or the admissibility of the numerical solutions. Here, the situation is different since we stay in the laboratory framework and compare the results with other well-known models.

In the present work, we wish to keep the models derivation particularly simple in order to present clear numerical comparisons. For this reason, we

do not mention the great difficulties encountered with a rigorous derivation of boundary conditions or admissible conditions. These aspects are challenging and out of the scope of the present study, here, we simply refer to existing results. The present communication is organized as follow. First of all, starting from a kinetic equation, the derivation of the M_1 and M_2 angular moments models is explained. The Navier-Stokes equations are also briefly recalled. Secondly, numerical simulations carried out in various collisional regimes are presented and illustrate the interest in considering angular moments models for rarefied gas dynamics applications. For each numerical test cases, the differences observed between the angular moments models and the well-known Navier-Stokes equations are discussed and compared with reference kinetic solutions.

2 Governing equations

We start by presenting the derivation of the angular moments models considered in this communication, namely the M_1 and M_2 angular moments model. Standard kinetic and Navier-Stokes equations are also briefly recalled in order to perform clear numerical comparisons.

2.1 M_1 angular moments model

The M_1 angular moments model can be easily derived starting from the kinetic equation

$$\partial_t f(t,x,v) + v.\nabla_x \left(f(t,x,v)\right) = C(f)(t,x,v). \tag{1}$$

Because of the complexity of the Boltzmann collisional operator, in this study, a simplified collisional operator is considered. More precisely this communication is carried out working with a standard BGK collision operator [17]

$$C(f)(t,x,v) = \nu(t,x)\left(M_f(t,x,v) - f(t,x,v)\right), \tag{2}$$

where M_f is the equilibrium Maxwellian distribution function

$$M_f(t,v,x) = n(t,x)\left(\frac{m}{2\pi k_b T(t,x)}\right)^{\frac{3}{2}} \exp\left(-\frac{m(v-u(t,x))^2}{2k_b T(t,x)}\right), \tag{3}$$

n the particles density, u the mean velocity, T the temperature and ν is a collisional frequency which will be specified. Expanding the velocity v as $v = \zeta\Omega$ (spherical coordinates), where ζ is the velocity modulus and Ω the velocity direction, the direct angular integration of the kinetic equation (1) against the weight function 1 and Ω leads to the following set of two equations

$$\begin{cases} \partial_t f_0 + \nabla.(\zeta f_1) = \nu(M_0 - f_0), \\ \partial_t f_1 + \nabla.(\zeta f_2) = \nu(M_1 - f_1), \end{cases} \tag{4}$$

where f_0, f_1 and f_2 are the first three angular moments of the particles distribution function defined by

$$f_0(\zeta) = \zeta^2 \int_{S^2} f(\Omega, \zeta) d\Omega, \quad f_1(\zeta) = \zeta^2 \int_{S^2} f(\Omega, \zeta) \Omega d\Omega,$$

$$f_2(\zeta) = \zeta^2 \int_{S^2} f(\Omega, \zeta) \Omega \otimes \Omega d\Omega.$$

It is important to notice that we keep the velocity modulus ζ as a variable (as the time t and space x). So, in practice, we are going to work with a grid for the velocity modulus. The terms M_0 and M_1 in the collisional part are obtained by angular integration of the collision operator (2)

$$M_0(t, x, \zeta) = \zeta^2 \int_{S^2} M_f(t, x, v) d\Omega, \quad M_1(t, x, \zeta) = \zeta^2 \int_{S^2} M_f(t, x, v) \Omega d\Omega.$$

Analytic expressions of M_0 and M_1 can be computed in terms of the velocity moments (macroscopic quantities) and one obtains

$$M_0 = n \frac{\zeta}{u} \sqrt{\frac{m}{2\pi k_b T}} \Big(\exp(\frac{2m\zeta u}{k_b T}) - 1 \Big) \exp\Big(- \frac{m(\zeta^2 + u^2)}{2k_b T} \Big),$$

$$M_1 = n \sqrt{\frac{m}{2\pi k_b T}} \Big(\frac{k_b T}{m} + \zeta u + \exp\left(\frac{2m\zeta u}{k_b T} \right) \Big) \Big(\frac{\zeta}{u} - \frac{k_b T}{m u^2} \Big) \exp\Big(- \frac{m(\zeta^2 + u^2)}{2k_b T} \Big).$$

Remark: One notices the division by the mean velocity u in the two previous equations. However we point out that the limit u tends to zero is not singular. Indeed, direct Taylor expansions give a finite value of M_0 and M_1 in the limit u tends to zero. In practice, these expansions are used to get rid of numerical issues encountered with small values of u.

Now, in order to close model (4), one needs to define the higher order moments f_2 as a function of f_0 and f_1. In the present work, following [27, 32, 10], the closure relation considered originates from an entropy minimization principle. The underlying distribution function f is obtained as a solution of the following minimization problem

$$\min_{f \geq 0} \left\{ \mathcal{H}(f) \ / \ \zeta^2 \int_{S^2} f(\Omega, \zeta) d\Omega = f_0(\zeta), \ \ \zeta^2 \int_{S^2} f(\Omega, \zeta) \Omega d\Omega = f_1(\zeta) \right\}, \tag{5}$$

where $\mathcal{H}(f)$ is the angular entropy defined by

$$\mathcal{H}(f) = \zeta^2 \int_{S^2} (f \ \ln \ f \ - \ f) d\Omega. \tag{6}$$

The solution of (5) writes [11, 28]

$$f(\Omega, \zeta) = \exp\left(a_0(\zeta) + a_1(\zeta) \, . \, \Omega \right), \tag{7}$$

where $a_0(\zeta)$ is a scalar and $a_1(\zeta)$ a real valued vector. Note that this closure function is an exponential because of the chosen entropy (similar to the Boltzmann entropy) (6). Once the form of the probability distribution function fixed the higher order moment f_2 can be computed as a function of f_0 and f_1 (see [9, 11])

$$f_2 = \left(\frac{1-\chi^{M1}(x)}{2} \bar{\bar{I}}d + \frac{3\chi^{M1}(x)-1}{2} \frac{f_1}{|f_1|} \otimes \frac{f_1}{|f_1|} \right) f_0, \tag{8}$$

with

$$\chi^{M1}(x) = (1+x^2+x^4)/3, \qquad x = f_1/f_0.$$

We define here the set of admissible states

$$\mathcal{A} = \Big((f_0, f_1) \in \mathbb{R} \times \mathbb{R}^3, \ f_0 \geq 0, \ \ |f_1| \leq f_0 \Big),$$

which gives the existence of a non-negative distribution function from the angular moments under consideration (see [34]). In the following, the collisional operator is computed implicitly because of the stiffness due to the collisional frequency ν (indeed we are going to perform simulations in all collisional regimes). For this purpose, following [4], we numerically solve the conservation laws associated to (4) before computing the collision operator term implicitly. The conservation laws in term of the angular moments write

$$\begin{cases} \partial_t n + \nabla . (nu) = 0, \\ \partial_t (nu) + \nabla . \left(\displaystyle\int_0^{+\infty} f_2 \zeta^2 d\zeta \right) = 0, \\ \partial_t E + \nabla . \left(\displaystyle\int_0^{+\infty} \frac{m}{2} f_1 \zeta^3 d\zeta \right) = 0, \end{cases} \tag{9}$$

where the particles density, the mean velocity, the total particles energy write in terms of the angular moments as follow

$$\begin{aligned} n(t,x) &= \int_{\mathbb{R}^3} f(t,x,v) dv = \int_0^{+\infty} f_0(t,x,\zeta) d\zeta, \\ u(t,x) &= \frac{1}{n(t,x)} \int_{\mathbb{R}^3} f(t,x,v) v dv = \frac{1}{n(t,x)} \int_0^{+\infty} f_1(t,x,\zeta) \zeta d\zeta, \\ E(t,x) &= \frac{m}{2} \int_{\mathbb{R}^3} f(t,x,v) v^2 dv = \frac{m}{2} \int_0^{+\infty} f_0(t,x,\zeta) \zeta^2 d\zeta. \end{aligned}$$

Before introducing the M_2 angular moments model we highlight the fact that the rigorous derivation of boundary conditions when working with moments models is a sensitive aspect and can be very challenging. This topic is clearly out the scope of the present study and we refer to [39, 24] where an analysis on this subject can be found. We believe it could also be applied in this context. In the following, for the numerical tests presented, the computational domain is chosen sufficiently large in order to avoid any numerical artifact due to some boundary interactions.

2.2 M_2 angular moments model

In this section the next order angular moments model named the M_2 angular is presented. This angular moments model reads

$$\begin{cases} \partial_t f_0 + \nabla.(\zeta f_1) = \nu(M_0 - f_0), \\ \partial_t f_1 + \nabla.(\zeta f_2) = \nu(M_1 - f_1), \\ \partial_t f_2 + \nabla.(\zeta f_3) = \nu(M_2 - f_2), \end{cases}$$

where f_3 is now the highest order angular moments defined by

$$f_3(\zeta) = \zeta^2 \int_{S^2} f(\Omega, \zeta) \Omega \otimes \Omega \otimes \Omega \, d\Omega.$$

As previously, the second order angular moments of the Maxwellian distribution function (3) can be computed numerically

$$M_2 = n \exp\left(-\frac{m(\zeta^2+u^2)}{2k_bT}\right) \exp\left(\frac{2m\zeta u}{k_bT}\right) \frac{\left(\zeta^2u^2 - 2\zeta u k_bT/m + 2k_b^2T^2/m^2\right) - \zeta^2u^2 - 2\zeta u k_bT/m - 2k_b^2T^2/m^2}{\sqrt{2\pi k_bT/m}\zeta u^3}.$$

Now using the minimum entropy principle as for the M_1 model, f_3 can be expressed as a function of f_0, f_1 and f_2. The derivation of the M_2 entropic closure and its associated admissibility conditions is a challenging issue far beyond the scope of the present study. Here we refer to [40] and [8] in which these two aspects have been addressed. In appendix, the M_1 and M_2 closure relations are given in the 1D case.

2.3 Navier-Stokes equations

Since numerical comparisons with the Navier-Stokes equations are presented in the following section, these equations are recalled in order to fix the notations. Well-known Navier-Stokes equations can be derived starting from the kinetic equation (1) introducing a fluid scaling and a standard Chapman-Enskog procedure [6, 5, 13]. In that case the particles distribution function under the Chapmann-Enskog ansatz writes

$$f = M_f + \varepsilon g, \qquad \int g \begin{pmatrix} 1 \\ v \\ v^2 \end{pmatrix} dv = 0, \tag{10}$$

where M_f is the Maxwellian equilibrium given in (2), ε is called the Knudsen number and g the equilibrium deviation. For clarity, we do not detail the

Chapman-Enskog procedure [6, 5, 13] and directly gives the resulting model with its closure relations

$$\begin{cases} \partial_t(mn) + \nabla.(mnu) = 0, \\ \partial_t(mnu) + \nabla.(mnu \otimes u + \Sigma(f)) = 0, \\ \partial_t E + \nabla.((E + \Sigma(f))\, u + q(f)) = 0, \end{cases} \tag{11}$$

where the stress tensor is defined by

$$\Sigma(f) = m \int_{\mathbb{R}^3} f(t,x,v)(v-u) \otimes (v-u) dv,$$

and the heat flux by

$$q(f) = \frac{m}{2} \int_{\mathbb{R}^3} f(t,x,v)(v-u)^2 (v-u) dv.$$

Now using the ansatz (10), the Chapman-Enskog procedure gives the Navier-Stokes closure relations

$$\Sigma(f) = \Sigma(M_f) + \varepsilon \Sigma(g), \qquad q(f) = q(M_f) + \varepsilon q(g),$$

where

$$\Sigma(M_f) = pI_d, \qquad q(M_f) = 0,$$

and the higher order terms

$$\Sigma(g) = -\mu\Big(\nabla u + (\nabla u)^t - \frac{2}{3}(\nabla.u) I_d\Big), \qquad q(g) = -\kappa \nabla T.$$

In addition, following the Chapmann-Enskog theory applied to a BGK model, the transport coefficients μ and κ are fixed in order to fit with the BGK model (2) (even if it is well known that a wrong Prandt number is recovered by the BGK model [17]) and write

$$\mu = \frac{p}{\nu}, \qquad \kappa = \frac{5pR}{2\nu}.$$

2.4 Numerical strategy

The HLL numerical scheme [22] is considered for the angular moments models and the Navier-Stokes equations. The HLL scheme considered here is one the simplest approximate Riemann solver (one intermediate state with two wave velocities to be defined). The intermediate state is set so that this approximate Riemann solver is consistent with the integral form of associated set of equations (Harten, Lax and Van Leer formalism). This numerical scheme is used extensively because of its strong stability properties (preservation of the admissible states and discrete entropy inequality

[3]). As already mentioned, implicit time discretisations are used for the collisional terms. Therefore when working with the M_1 and M_2 moments models, we start by solving the conservation equations to access to the updated macroscopic quantities, then the collisional operators are shaped and the new moments are finally computed. In order to perform rigorous numerical comparisons, second-order accuracy enhancements based on standard second-order Van Leers slope limiter [26] methods are used. This leads to a significant improvement of the numerical solutions which is mandatory since converged numerical results are required in order to perform fair model comparisons.

3 Numerical test cases

In this section, numerical simulations carried out in different collisional regimes are presented. For each numerical test case, the differences observed between the angular moments models and the Navier-Stokes equations are discussed and compared with reference BGK kinetic solutions.

3.1 A regular test case

The first numerical experiment considers the relaxation process of an hot spot in different collisional regimes. The initial probability distribution function writes

$$f^{\text{ini}}(x,v) = \left(\frac{m}{2\pi k_b T^{\text{ini}}(x)}\right)^{\frac{3}{2}} \exp\left(-\frac{mv^2}{2k_b T^{\text{ini}}(x)}\right),$$

where

$$T^{\text{ini}}(x) = 1 - \exp\left(-x^2/(2L)\right),$$

and $L = 40$. The space domain is $[-L, L]$. The velocity grid used for the kinetic reference is $[-8, 8]^3$ with 64 cells for each grid while the velocity modulus used for the angular moments model is $[0, 8]$ with 32 cells. For all models, the space cells number is 400.

a. Fluid regime
On Figure 1, the density (top left), speed (top right), temperature (bottom left) and heat flux (bottom right) profiles are displayed at time $t = 15$ in the case $\tau = 1/\nu = 0$. It is observed that the four models give exactly the same solution. This was expected since all the models are able to capture Maxwellian equilibrium distributions (fluid regimes). This validates the implementation and the accuracy of the numerical strategy chosen. This also shows that accurate and fair comparisons are feasible.

b. Close fluid and rarefied regimes
On Figure 2, density (top left), speed (top right), temperature (bottom left) and heat flux (bottom right) profiles are displayed at time $t = 5$ in the case $\tau = 1/\nu = 1$. It is observed that the results produced by the M_1 model (in green) are very slightly different to the ones given by the other models which remain close. On Figure 3, the profiles are displayed at time $t = 5$ in the case $\tau = 1/\nu = 100$ (rarefied regime). It is observed that the Navier-Stokes profiles dropped completely compared to the moments models and the kinetic reference. In this regime one remarks that the M_1 and M_2 moments models are much more accurate than the Navier-Stokes equations. The angular M_1 gives reasonably good results while the M_2 moments model is very accurate and remains very close to the kinetic reference solutions.

c. Very rarefied regime
On Figure 4, density (top left), speed (top right), temperature (bottom left) and heat flux (bottom right) profiles are displayed at time $t = 5$ in the case $\tau = 1/\nu = 10^4$. In this very rarefied regime, it is observed that the Navier-equations profiles are completely wrong (completely diffused). The M_1 results are still acceptable while the M_2 moments model remains very accurate.

3.2 Discontinuous test case: Riemann problem

We now consider a Riemann problem in different collisional regimes. The initial probability distribution function is the following

$$f^{\text{ini}}(x,v) = n^{\text{ini}}(x)\left(\frac{m}{2\pi k_b T^{\text{ini}}(x)}\right)^{\frac{3}{2}} \exp\left(-\frac{mv^2}{2k_b T^{\text{ini}}(x)}\right),$$

where

$$n^{\text{ini}}(x) = \begin{cases} 1.0 & \text{if} \quad x < 0, \\ 0.125 & \text{if} \quad x > 0, \end{cases}$$

and

$$T^{\text{ini}}(x) = \begin{cases} 1.0 & \text{if} \quad x < 0, \\ 0.8 & \text{if} \quad x > 0. \end{cases}$$

The space domain is $[0, 1]$. The velocity grid used for the kinetic reference is $[-8, 8]^3$ with 64 cells for each grid while the velocity modulus used for the angular moments model is $[0, 8]$ with 32 cells. For all models, the space cells number is 400.

a. Fluid regime
On Figure 5, the density (top left), speed (top right), temperature (bottom

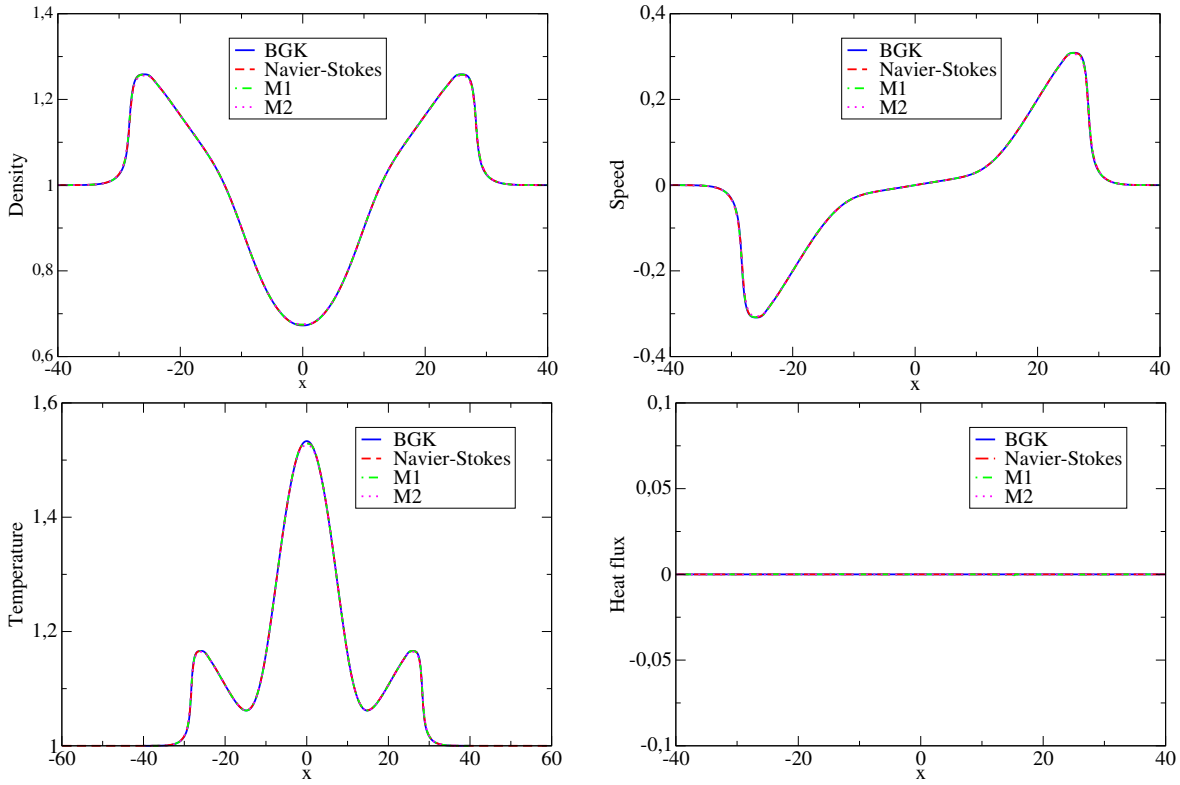

Figure 1: Density (top left), speed (top right), temperature (bottom left), heat flux (bottom right) profiles in the case $\tau = 1/\nu = 0$ (fluid regime) at time $t = 15$.

left) and heat flux (bottom right) profiles are displayed at time $t = 0.25$ in the case $\tau = 1/\nu = 0$ (fluid regime). It is observed that the four models give exactly the same solution. As with the previous test case, this was expected since all the models capture Maxwellian equilibrium distributions.

b. Intermediate regimes

On Figure 6, density (top left), speed (top right), temperature (bottom left) and heat flux (bottom right) profiles are displayed at time $t = 0.1$ in the case $\tau = 1/\nu = 10^{-2}$. As observed with the previous test case, it is observed that the results produced by the M_1 model are slightly different to the ones given by the other models which remain close. On Figure 7, the profiles are displayed at time $t = 0.1$ in the case $\tau = 1/\nu = 10^{-1}$ (so that the collisional frequency is decreased very slowly). It is observed that the Navier-Stokes profiles have started to drop. At this intermediate collisional level it is hard to decide which model between the M_1 and the Navier-Stokes is the best. It is also observed that the M_2 results are not perfect (small differences are observed with the kinetic) but still remains very accurate compared to M_1

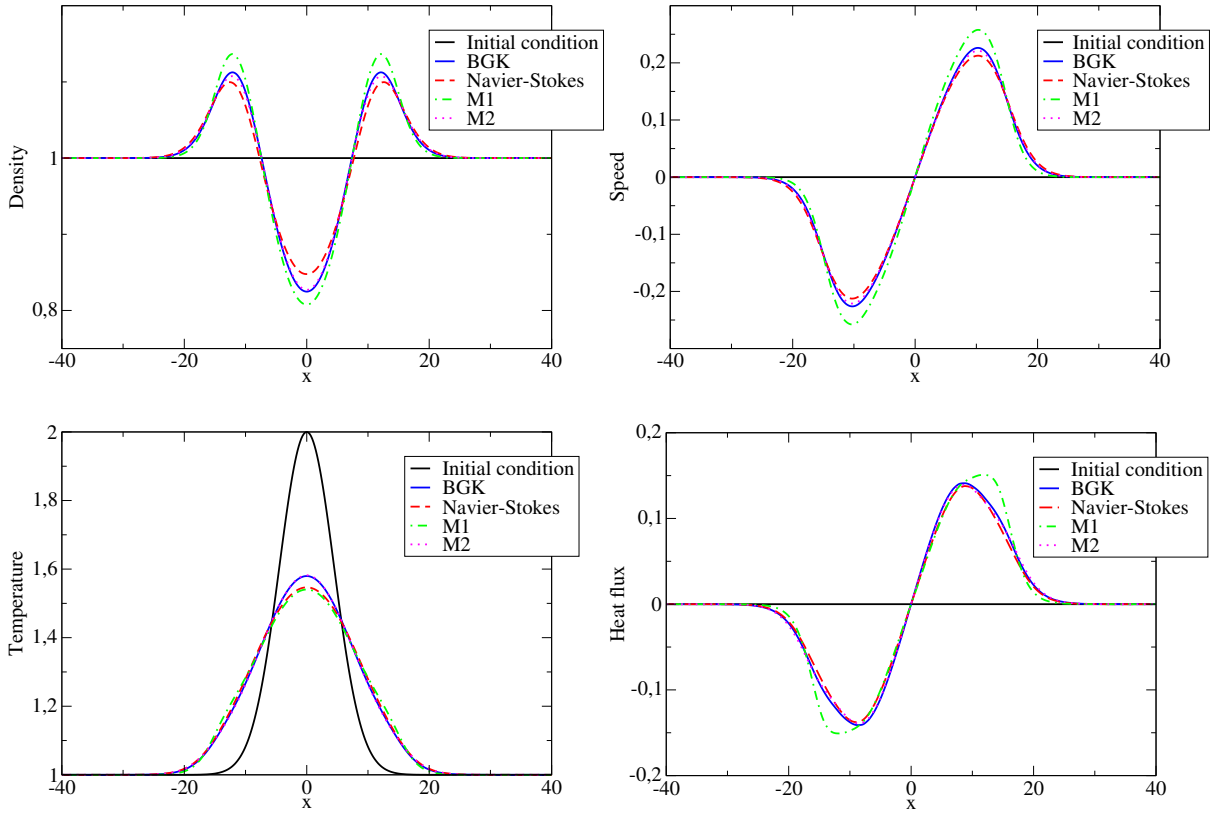

Figure 2: Representation of the density (top left), speed (top right), temperature (bottom left), heat flux (bottom right) in the case $\tau = 1/\nu = 1$ (close fluid regime) at time $t = 5$.

and Navier-Stokes.

c. Intermediate-rarefied regimes
On Figure 8, density (top left), speed (top right), temperature (bottom left) and heat flux (bottom right) profiles are displayed at time $t = 0.1$ in the case $\tau = 1/\nu = 1$ (still intermediate collisional regimes). Even if the fluid is not really in a rarefied regime, it is observed that the Navier-equations profiles are completely wrong. Here, the M_1 results are much more accurate and the M_2 results are very good (but not perfect). We do not push the numerical tests into more rarefied regimes since the Navier-Stokes gets even worse while the angular moments keep the same level of accuracy.

3.3 Discontinuous test case: double shock wave problem

We now focus on shock waves profiles in different collisional regimes with a special focus on the heat flux profiles. The fluid velocity is initialized so

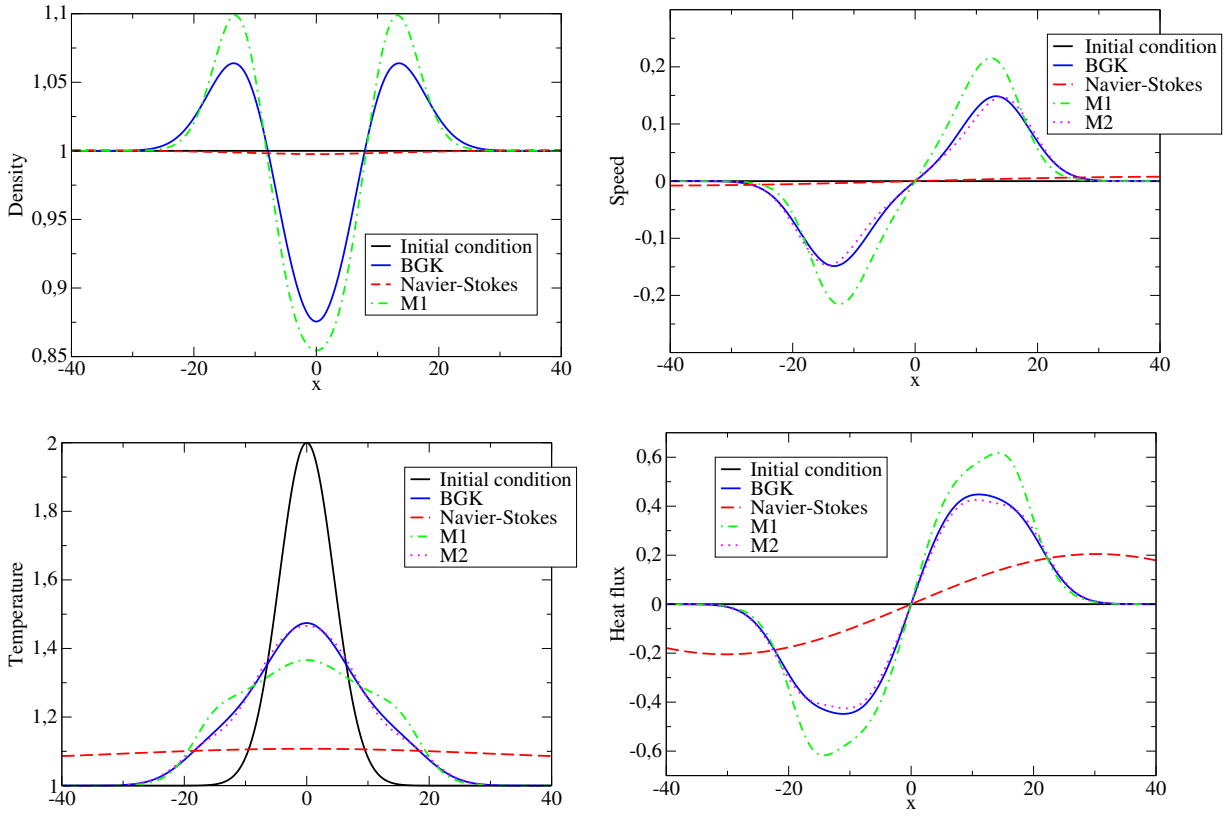

Figure 3: Representation of the density (top left), speed (top right), temperature (bottom left), heat flux (bottom right) in the case $\tau = 1/\nu = 100$ (rarefied regime) at time $t = 5$.

that two shock waves are created and propagate in opposite directions. The initial probability distribution function is the following

$$f^{\text{ini}}(x,v) = n^{\text{ini}}(x)\left(\frac{m}{2\pi k_b T^{\text{ini}}(x)}\right)^{\frac{3}{2}} \exp\left(-\frac{m(v-u^{ini})^2}{2k_b T^{\text{ini}}(x)}\right),$$

where

$$n^{\text{ini}}(x) = \begin{cases} 1.0 & \text{if} \quad x < 0, \\ 1.0 & \text{if} \quad x > 0, \end{cases}$$

$$u^{\text{ini}}(x) = \begin{cases} 1.0 & \text{if} \quad x < 0, \\ -1.0 & \text{if} \quad x > 0, \end{cases}$$

and

$$T^{\text{ini}}(x) = \begin{cases} 1.0 & \text{if} \quad x < 0, \\ 1.0 & \text{if} \quad x > 0. \end{cases}$$

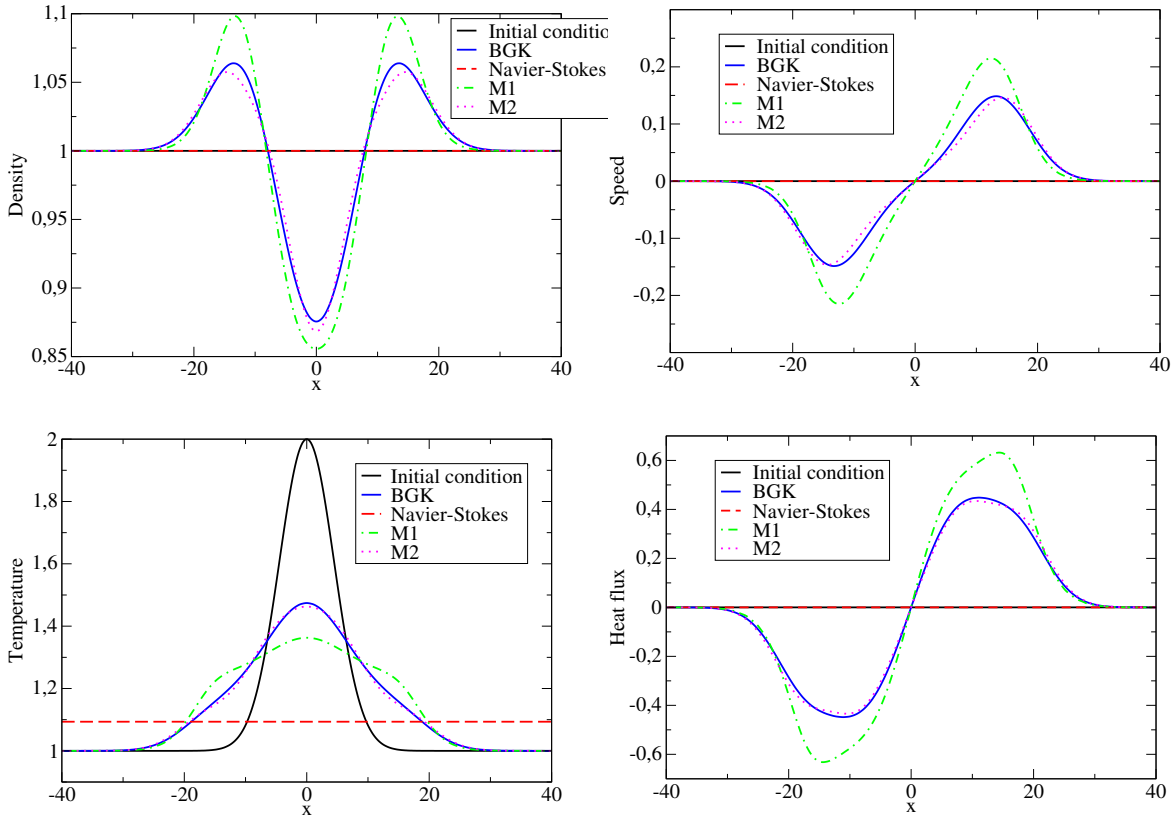

Figure 4: Representation of the density (top left), speed (top right), temperature (bottom left), heat flux (bottom right) in the case $\tau = 1/\nu = 10^4$ (strongly rarefied regime) at time $t = 5$.

The space domain is $[0, 1]$. The velocity grid used for the kinetic reference is $[-8, 8]^3$ with 64 cells for each grid while the velocity modulus used for the angular moments model is $[0, 8]$ with 32 cells. For all models, the space cells number is 400.

a. Fluid regime

On Figure 9, the density (top left), speed (top right), temperature (bottom left) and heat flux (bottom right) profiles are displayed at time $t = 0.2$ in the case $\tau = 1/\nu = 0$ (fluid regime). It is observed that the four models give exactly the same solution. As with the previous test case, this was expected since all the models capture Maxwellian equilibrium distributions.

b. Close fluid regime / intermediate regime

On Figure 10, density (top left), speed (top right), temperature (bottom left) and heat flux (bottom right) profiles are displayed at time $t = 0.1$ in the case $\tau = 1/\nu = 10^{-1}$. In this intermediate regime (still close of the

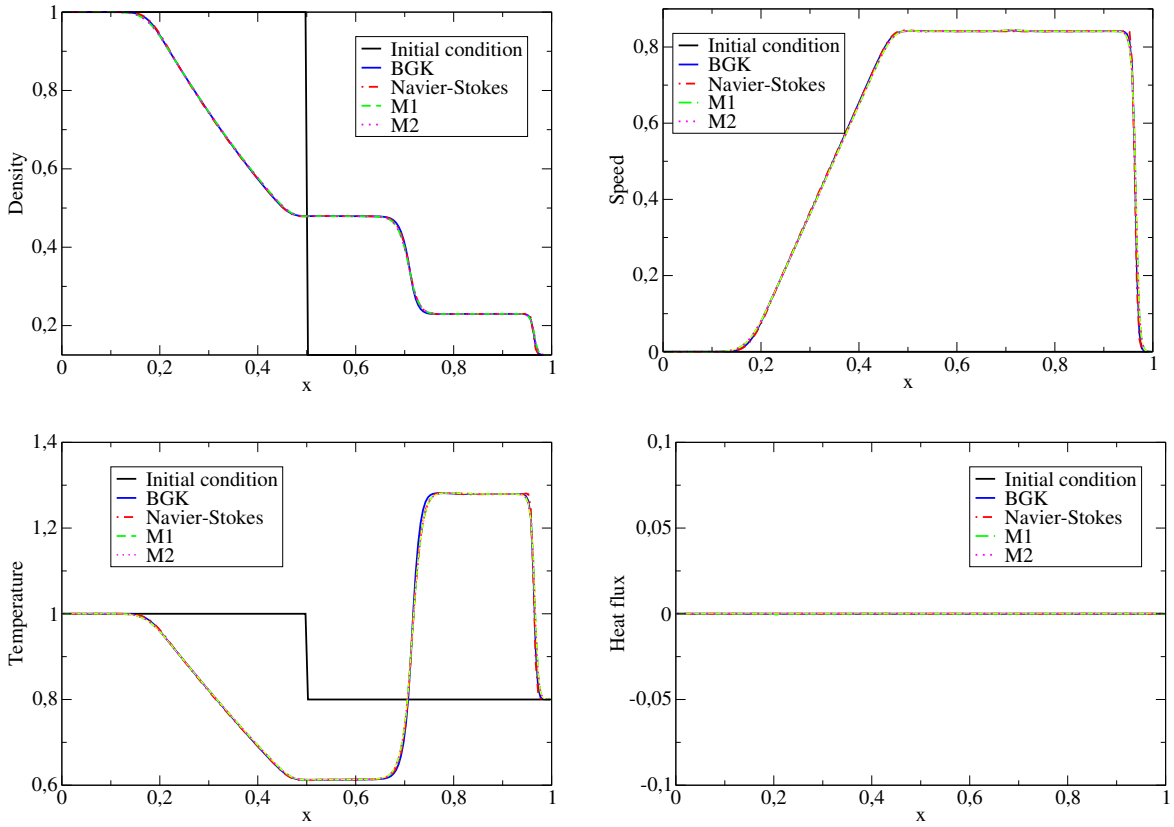

Figure 5: Representation of the density (top left), speed (top right), temperature (bottom left), heat flux (bottom right) in the case $\tau = 1/\nu = 0$ (fluid regime) at time $t = 0.25$.

fluid regime) it is observed that the M_1 model is the most inaccurate clearly overestimating the density profiles. When looking at higher order moments quantities such as the heat flux, it is remarked that the M_1 heat flux profile is too sharp while the Navier-Stokes heat flux under-estimates the solution. The M_2 profiles and the kinetic ones are very close. As already observed in this close fluid regime that M_1 seems less accurate than Navier-Stokes while M_2 is by far the most accurate reduced models.

c. Intermediate / rarefied regimes

On Figure 11, density (top left), speed (top right), temperature (bottom left) and heat flux (bottom right) profiles are displayed at time $t = 0.1$ in the case $\tau = 1/\nu = 1$ (still intermediate collisional regimes). Here also, even if the flow is not really rarefied, it is observed that the Navier-equations profiles are completely wrong. Even if the M_1 results are not perfect they are rather accurate and M_2 is very accurate. As before, we do not push the numerical tests into rarefied regimes since the Navier-Stokes results gets

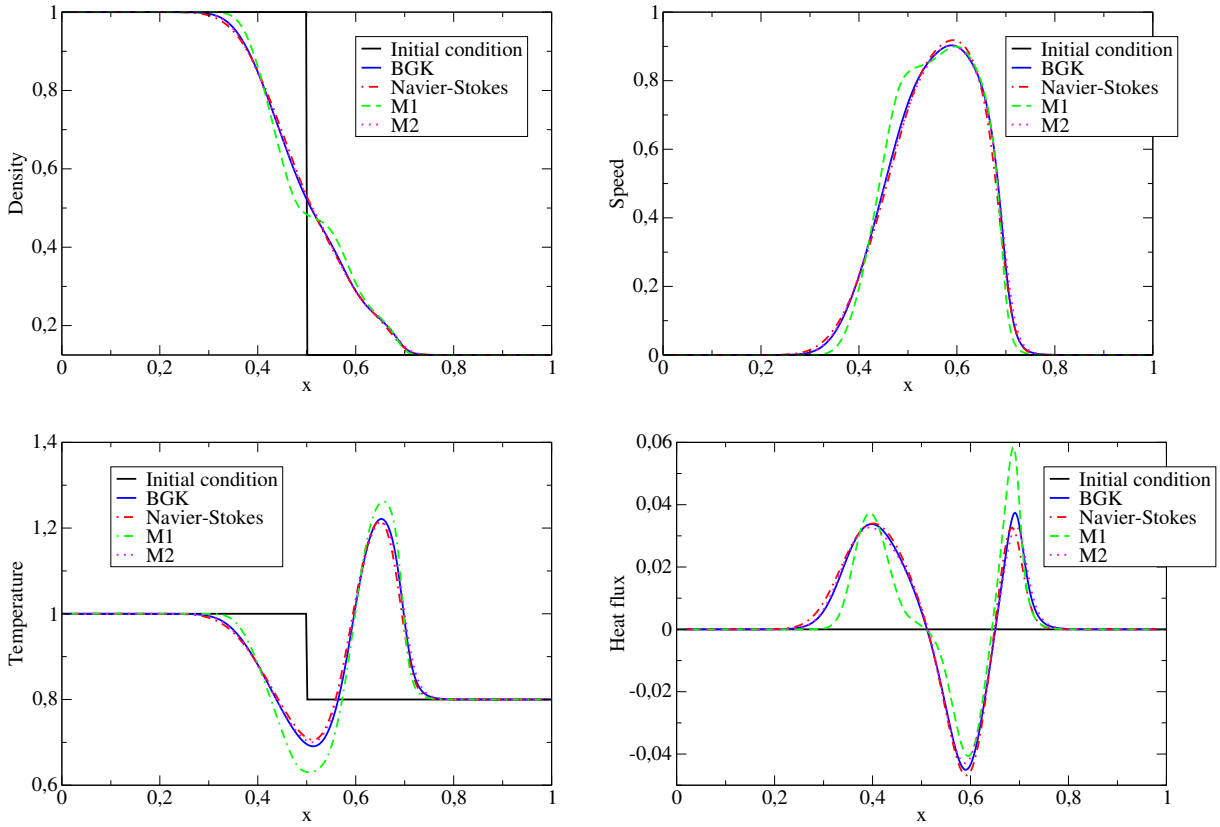

Figure 6: Representation of the density (top left), speed (top right), temperature (bottom left), heat flux (bottom right) in the case $\tau = 1/\nu = 10^{-2}$ (close of fluid regime) at time $t = 0.1$.

even worse while the angular moments keep the same level of accuracy. This clearly shows the interest in considering angular moments models to capture accurate heat fluxes especially in rarefied regimes.

3.4 Stationary shock wave

The last numerical test case we consider is taken from [31] and consists in studying the length of a stationary shock for different upstream flows. At initial time, one starts with Maxwellian distribution functions and the upstream flow (left in-going flow) is set as follow

$$\begin{cases} \rho^L = mn^L = 66.3 \cdot 10^{-7}, \\ u^L = M\sqrt{\gamma R T^L}, \\ T^L = 293, \end{cases}$$

where M is the Mach number (which will be made vary) and the physical parameters are $\gamma = 5/3$ and $R = k_b/m = (1.38054 \cdot 10^{-23})/(66.3 \cdot 10^{-27})$.

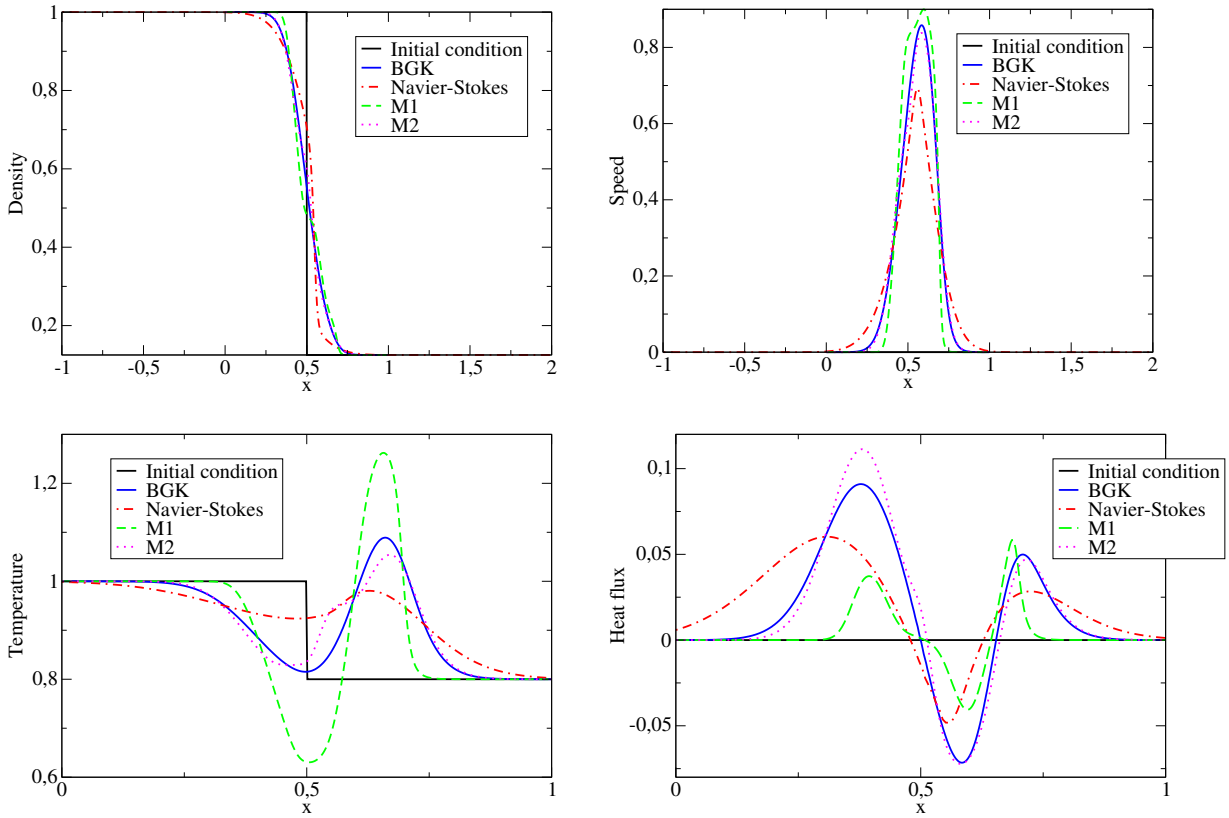

Figure 7: Representation of the density (top left), speed (top right), temperature (bottom left), heat flux (bottom right) in the case $\tau = 1/\nu = 10^{-1}$ at time $t = 0.1$.

The downstream flow is fixed using the Rankine-Hugoniot conditions (stationary shock). In addition a non-constant collisional period is considered and depends on density and temperature as followed

$$\tau = 1/\nu = 1.08 \cdot 10^{-9} \cdot (T^{-0.19})/n.$$

The width of the computational domain is 0.5 and a grid of 400 cells is used. The velocity modulus used for the angular moments model is $[0, 5000]$ with 500 cells. For each value of the Mach number, the length of the stationary shock wave is different. Indeed, by changing the upstream velocity one also modifies the collisional frequency and the corresponding shock length. The results obtained with the angular models are displayed in Figure (12) and compared with those given in [31] (for Navier-Stokes and BGK). The inverse of the shock thickness is given for different values of the Mach number. First of all, the results presented in (12) show that the kinetic BGK model (red circles) is able to reproduce the correct shock thickness for all the Mach numbers (good agreement with the experiments see [31]). On the other hand,

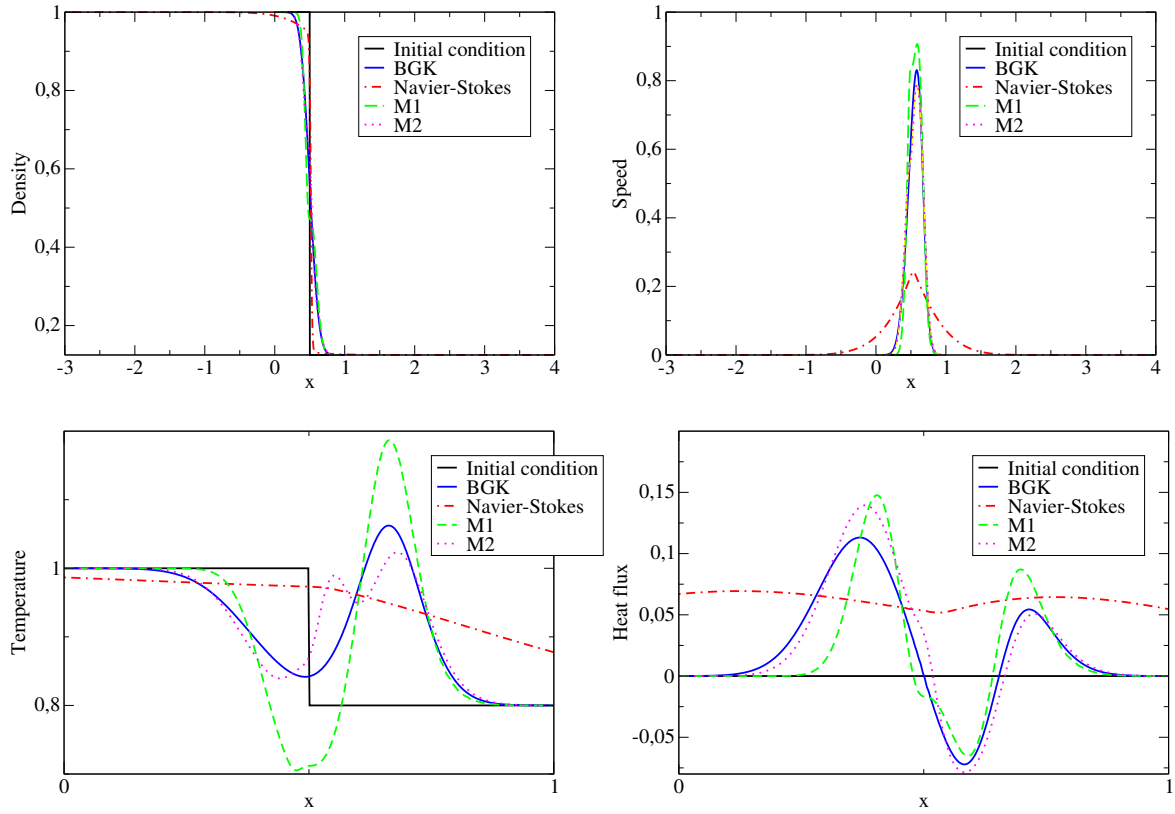

Figure 8: Representation of the density (top left), speed (top right), temperature (bottom left), heat flux (bottom right) in the case $\tau = 1/\nu = 1$ (intermediate regimes) at time $t = 0.1$.

it is observed that the Navier-Stokes results (black dash lines) are only valid for small Mach number values (≈ 1). Concerning the angular moments models, it is remarked that the M_1 model (in green) underestimates the shock profiles for all the different Mach number. For small and intermediate values of the Mach number ($\approx 1 - 6$), the Navier-stokes results are more accurate than the ones obtained with the M_1 model while for large Mach numbers the Navier-Stokes and M_1 results are comparable. On the contrary it is observed that the M_2 model is always much more accurate than the M_1 model and the Navier-Stokes equations and is close to the BGK and the experiments.

4 Numerical costs

The numerical costs greatly depends on the number of cells used for the velocity modulus grid in addition to the size of the grid (which constrains the CFL condition). Similarly, kinetics codes are strongly impacted by the

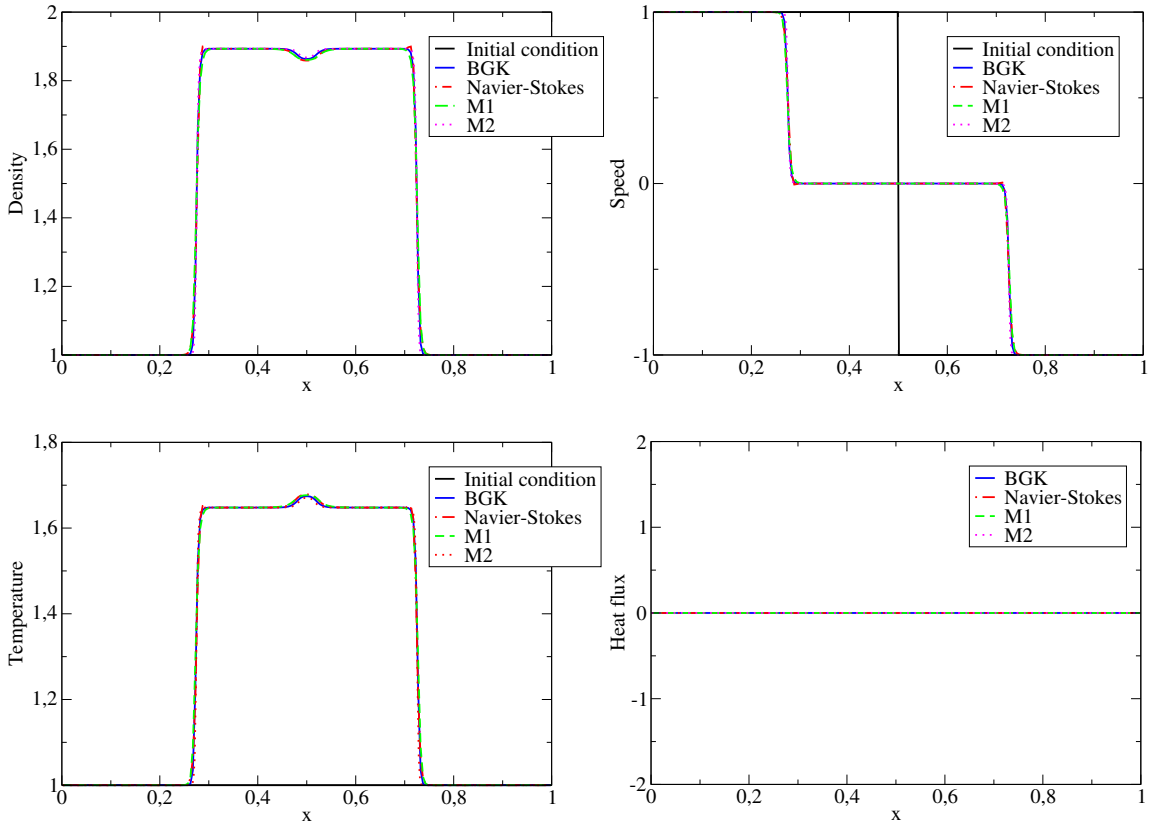

Figure 9: Representation of the density (top left), speed (top right), temperature (bottom left), heat flux (bottom right) in the case $\tau = 1/\nu = 0$ (fluid regime) at time $t = 0.2$.

number of cells used for the velocity grids in addition to the size of the grid. Typically, for the numerical test case presented, it is observed the M_1 code is about three times slower than the Navier-Stokes code (this is expected since a velocity modulus grid is used). The M_2 code is about six times longer than the Navier-Stokes code while the reference kinetic code is much longer (more than twenty times longer). Again, we emphasize that the numerical costs strongly depends on the configuration studied. However, even if the angular moments models codes are more expensive than the Navier-Stokes code they are always much faster than the kinetic reference ones.

5 Conclusion and perspectives

In the present communication, angular moments models based on a minimum entropy problem have been presented for rarefied gas dynamics applications. The numerical simulations carried out in various collisional regimes illustrate the interest in considering angular moments models for rarefied

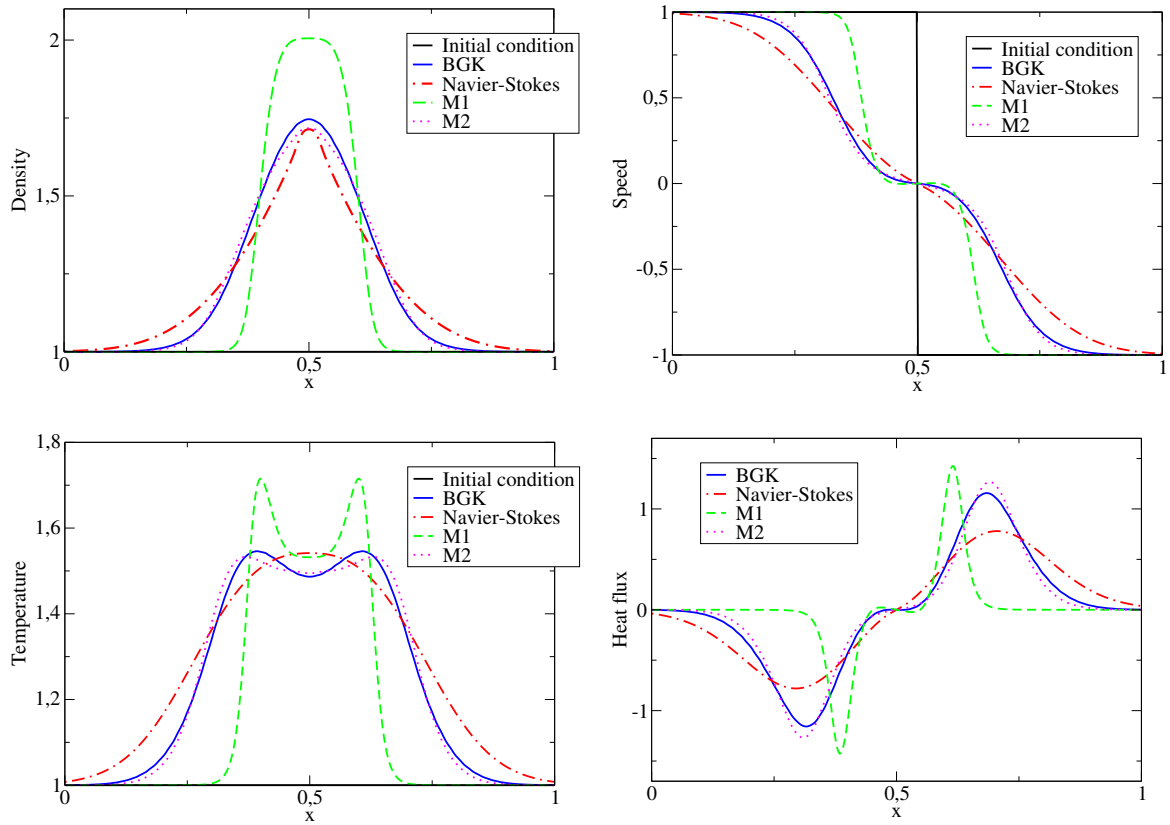

Figure 10: Representation of the density (top left), speed (top right), temperature (bottom left), heat flux (bottom right) in the case $\tau = 1/\nu = 10^{-1}$ at time $t = 0.1$.

gas dynamics applications. In particular, the comparisons with the Navier-Stokes equation and the kinetic reference clearly point out the accuracy of angular models in rarefied regimes. As perspectives the derivation of rigorous boundary conditions will be investigated. In addition numerical comparisons in a 2D space geometry can also be considered.

Acknowledgments

The author thanks B. Dubroca for many interesting discussions on the subject.

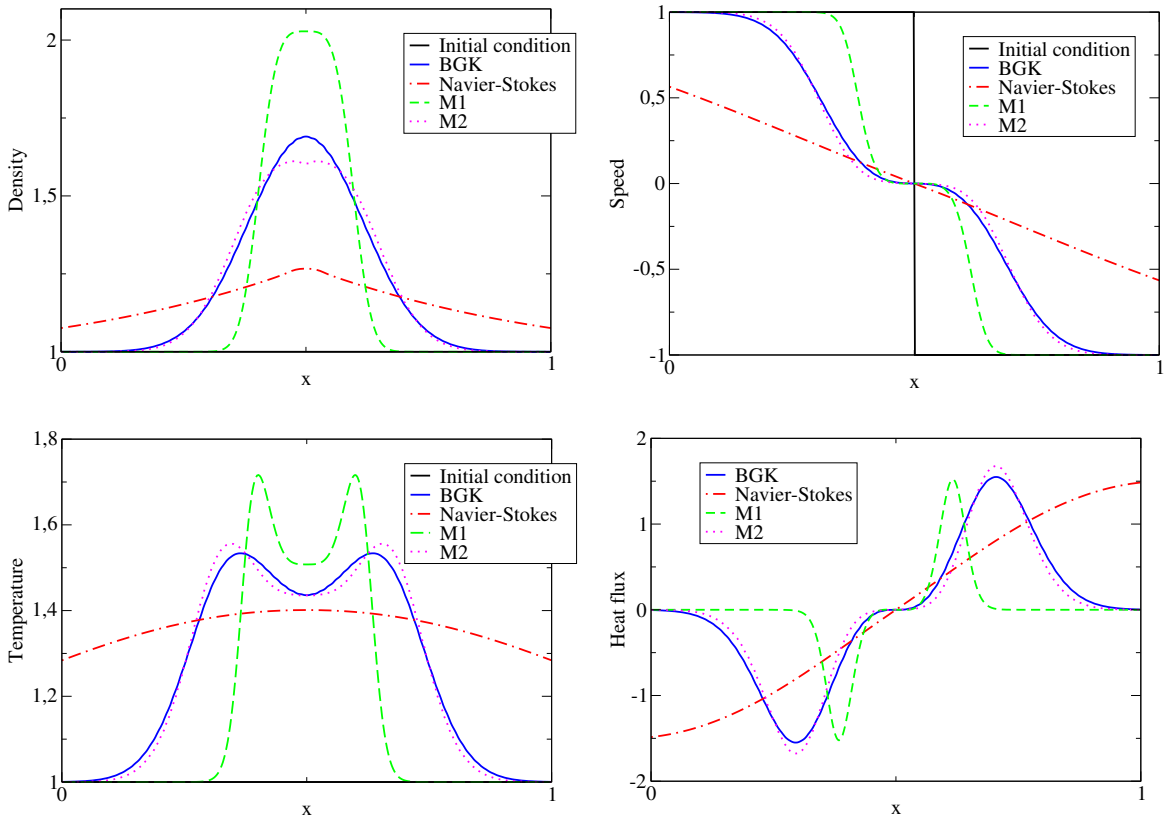

Figure 11: Representation of the density (top left), speed (top right), temperature (bottom left), heat flux (bottom right) in the case $\tau = 1/\nu = 1$ at time $t = 0.1$.

6 Appendix

6.1 Closure relations

In this section the closure relations used for the M_1 and M_2 models are provided. We highlight that the derivation of the closure relations is challenging and we refer to [21, 40] for the procedure details which are clearly out the scope of the present document. Here, the closure relations used to perform the numerical comparisons are simply given.

a. M_1 closure

In the 1D framework the approximated M_1 closure considered simply reads

$$f_2(x) = \chi^{M1}(x) f_0, \qquad \chi^{M1}(x) = (1 + x^2 + x^4)/3, \qquad x = f_1/f_0.$$

b. M_2 closure

The M_2 closure given here is taken from [40]. In the 1D framework it writes

$$f_3(x_1, x_2) = \chi^{M2}(x_1, x_2) f_0, \qquad x_1 = f_1/f_0, \qquad x_2 = f_2/f_0.$$

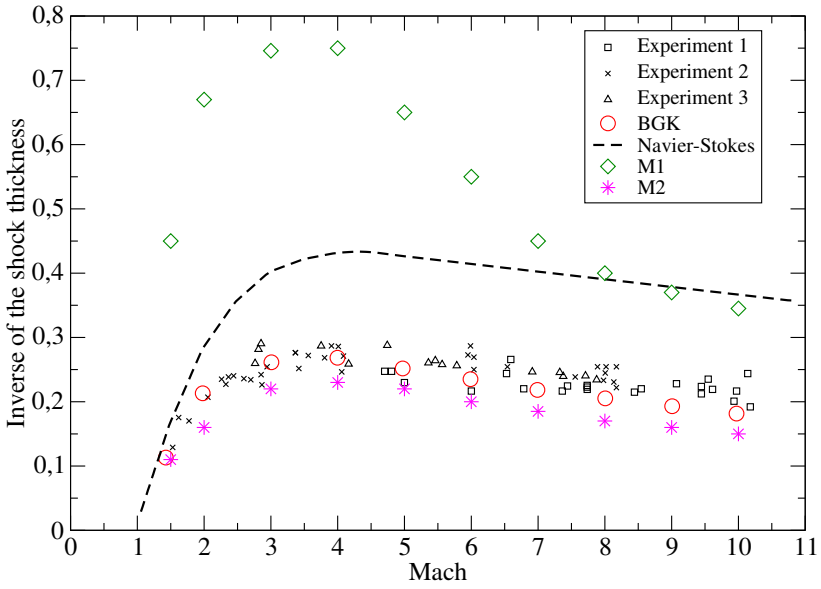

Figure 12: Representation of the inverse of the shock thickness as function of the Mach number (speed of the in-going flow).

where χ^{M2} is defined as follows

$$\chi^{M2}(x,y) = b_-(x,y)\theta_3(x,y) + b_+(x,y)(1-\theta_3(x,y)).$$

where

$$b_-(x,y) = -y + \frac{(x+y)^2}{(1+x)}, \qquad b_+(x,y) = y - \frac{(x-y)^2}{(1+x)},$$

and the coefficient $\theta_3 \in [0,1]$ is defined by

$$\theta_3(x,y) = E\left((T_1,0),\left(T_2,\frac{\chi_2(x)-x^2}{1-x^2}\right),(T_3,1)\right)(y) + Z\left(0,\frac{\chi_2(x)-x^2}{1-x^2},1\right)(y)Q_1(x,y).$$

The following notations have been used: The polynomial of degree two interpolating the values A, B and C at the points a, b and c is denoted E, and Z denotes the polynomial of degree three which is zero in a, b and c:

$$E((A,a),(B,b),(C,c))(x) = A\frac{x-b}{a-b}\frac{x-c}{a-c} + B\frac{x-a}{b-a}\frac{x-c}{b-c} + C\frac{x-a}{c-a}\frac{x-b}{c-b},$$

$$Z(a,b,c)(x) = (x-a)(x-b)(x-c).$$

The coefficient χ_2 is defined by

$$\chi_2(x) = x^2\theta_1(x) + (1-\theta_1(x)),$$

with

$$\theta_1(x) = x^2 + \frac{2}{3}(1-x^2) + x^2(1-x^2)(c_0 + c_1 x^2 + c_2 x^4),$$

where $c_0 = -0.0954823981432433$, $c_1 = 0.229069986304953$ and $c_2 = 0.0344846229504588$. Q_1 is a polynomial of x and y. Its coefficients are chosen such that the discrete $L2$ distance between the approximated and the exact χ^{M_2} (computed by solving the M_2 minimization problem for 10^4 values of (x_1, x_2), given by 100 values of x equally distributed in $[0,1]$ and 100 of y equally distributed in $[0,1]$) is minimized (see [40]). It is defined by

$$Q_1(x,y) = \sum_{i=1}^{n=8} \sum_{j=1}^{n=8} a_{ij} x^{i-1} y^{j-1},$$

where a_{ij} refers to the element in row i and column j of matrix A:

$$\begin{pmatrix}
1.2560236 & 0.055167449 & 0.26278138 & 1.0683350 & 0.59814167 & -0.64518803 & -1.0633483 & 0.88934267 \\
-0.68894512 & 0.31161185 & 1.2786018 & -0.31163011 & -2.9649475 & -4.5186998 & -3.3074111 & 1.6029077 \\
0.12662825 & 2.5077746 & 3.9023476 & 3.0134469 & 1.6566437 & 1.6814247 & 4.2771384 & 9.9743799 \\
-4.4012020 & -2.2244757 & -1.6449706 & -2.7851846 & -4.0598413 & -4.0955056 & -2.0870623 & 2.2694786 \\
-0.84307105 & 0.56713889 & -0.010068180 & -2.0311387 & -4.1712022 & -5.4023878 & -5.1525837 & -3.2239003 \\
4.1781734 & 6.0798187 & 5.4981218 & 3.3301219 & 0.72710695 & -1.4776834 & -2.8201005 & -3.1245525 \\
1.1299516 & 5.7191442 & 7.0928923 & 6.3554499 & 4.5787199 & 2.5179169 & 0.61766327 & -0.91306843 \\
-16.015241 & -6.4386305 & -1.0307863 & 1.4581785 & 2.0925223 & 1.6270272 & 0.54281204 & -0.88389340
\end{pmatrix}$$

In addition

$$T_1 := \frac{b_+ - \kappa_1}{b_+ - b_-}(x,0), \quad T_2 := \frac{b_+ - \kappa_1}{b_+ - b_-}\left(x, \frac{\chi_2(x) - x^2}{1-x^2}\right), \quad T_3 := \frac{b_+ - \kappa_1}{b_+ - b_-}(x,1).$$

where

$$\kappa_1(x,0) = x^3, \quad \kappa_1\left(x, \frac{\chi_2(x) - x^2}{1-x^2}\right) = \chi_3(x), \quad \kappa_1(x,1) = x,$$

with

$$\chi_3(x) = b_-(x, \chi_2(x))\theta_2(x) + b_+(x, \chi_2(x))(1 - \theta_2(x)),$$

and

$$\theta_2(x) = \frac{1}{2} + x\left(-\frac{1}{2} + (1-x^2)(d_0 + d_1 x^2 + d_2 x^4)\right),$$

with $d_0 = 0.386143553495150$, $d_1 = 0.488034553677475$ and $d_2 = 0.681343955348390$.

6.2 Numerical strategy

The numerical strategy used for the angular moments models is now presented. We write the discrete quantities with an index i for the space discretisation and an index j for the modulus velocity discretisation. The time step, the space step and the velocity modulus step are respectively denoted

Δt, Δx and $\Delta\zeta$.

a. Discrete M_1 model

In the 1D slab the HLL numerical scheme used for the M_1 model (4) (in the simplified case of opposite wave velocities in the underlying approximate Riemann solver) with implicit collisional terms writes

$$\begin{aligned}
&\frac{f_{0ij}^{n+1}-f_{0ij}^{n}}{\Delta t}+\frac{f_{1i+1/2j}^{n}-f_{1i-1/2j}^{n}}{\Delta x}=\nu_i^{n+1}(M_{0ij}^{n+1}-f_{0ij}^{n+1}),\\
&\frac{f_{1ij}^{n+1}-f_{1ij}^{n}}{\Delta t}+\frac{f_{2i+1/2j}^{n}-f_{2i-1/2j}^{n}}{\Delta x}=\nu_i^{n+1}(M_{1ij}^{n+1}-f_{1ij}^{n+1}),
\end{aligned} \tag{12}$$

where the numerical fluxes used are defined by

$$\begin{cases}
f_{1,i+1/2j}^{n}=\dfrac{\zeta_j}{2}(f_{1i+1j}^{n}+f_{1ij}^{n})-\dfrac{\zeta_j}{2}(f_{0i+1j}^{n}-f_{0ij}^{n}),\\
f_{2,i+1/2j}^{n}=\dfrac{\zeta_j}{2}(f_{2i+1j}^{n}+f_{2ij}^{n})-\dfrac{\zeta_j}{2}(f_{1i+1j}^{n}-f_{1ij}^{n}).
\end{cases}$$

It is well known that this numerical scheme preserves the admissibility of the numerical solution that under CFL condition

$$\Delta t\leq\frac{\Delta x}{||\zeta||_\infty}.$$

The same procedure is used for the M_2 model.

b. Discretisation of the conservation laws

In order to compute the terms M_{0i}^{n+1}, M_{1i}^{n+1} and the collisional frequencies ν_i^{n+1}, a suitable discretisation of the conservation laws (9) is required. Integrating (at the discrete level) the numerical scheme (12) leads to the discrete continuity equation

$$\frac{n_i^{n+1}-n_i^{n}}{\Delta t}+\sum_j\frac{f_{1i+1/2j}^{n}-f_{1i-1/2j}^{n}}{\Delta x}\Delta\zeta=0.$$

The discrete momentum equation is obtained by multiplying the second equation of (12) by $\zeta_j\Delta\zeta$ and adding in j

$$\frac{(nu)_i^{n+1}-(nu)_i^{n}}{\Delta t}+\sum_j\frac{f_{2i+1/2j}^{n}-f_{2i-1/2j}^{n}}{\Delta x}\zeta_j\Delta\zeta=0.$$

The energy equation is obtained by multiplying the first equation of (12) by $\zeta_j^2\Delta\zeta/2$

$$\frac{E_i^{n+1}-E_i^{n}}{\Delta t}+\sum_j\frac{f_{1i+1/2j}^{n}-f_{1i-1/2j}^{n}}{\Delta x}\frac{\zeta_j^2}{2}\Delta\zeta=0.$$

References

[1] G.W. Alldredge, C.D. Hauck, and A.L. Tits. High-order entropy-based closures for linear transport in slab geometry II: A computational study of the optimization problem. SIAM Journal on Scientific Computing Vol. 34-4 (2012), pp. B361-B391.

[2] C. Berthon, P. Charrier, and B. Dubroca. An HLLC Scheme to Solve The M1 Model of Radiative Transfer in Two Space Dimensions. Journal of Scientific Computing, Vol. 31, No. 3, (2007).

[3] F. Bouchut. Nonlinear Stability of Finite Volume Methods for Hyperbolic Conservation Laws, and Well-Balanced Schemes for sources. Frontiers in Mathematics series, Birkhauser. (2004).

[4] S. Brull and L. Mieussens. Local discrete velocity grids for deterministic rarefied flow simulations. J. Comput. Phys., 266(1), 22-46 (2014).

[5] S. Chapman. On the Law of Distribution of Molecular Velocities, and on the Theory of Viscosity and Thermal Conduction, in a Non-Uniform Simple Monatomic Gas. Phil. Trans. Roy. Soc. London 216 (1916) 279.

[6] S. Chapman and T. G. Cowling. The Mathematical Theory of Non-Uniform Gases. Cambridge University Press, Cambridge, England, 1995.

[7] P. Charrier, B. Dubroca, G. Duffa, and R. Turpault. Multigroup model for radiating flows during atmospheric hypersonic re-entry. Proceedings of International Workshop on Radiation of High Temperature Gases in Atmospheric Entry, pp. 103110. Lisbonne, Portugal. (2003).

[8] A. Decoster. Personnal communication (2018).

[9] B. Dubroca, J.-L. Feugeas, and M. Frank. Angular moment model for the Fokker-Planck equation. European Phys. Journal D, 60, 301, (2010).

[10] B. Dubroca and J.L. Feugeas. Entropic moment closure hierarchy for the radiative transfert equation. C. R. Acad. Sci. Paris Ser. I, 329 915, (1999).

[11] B. Dubroca and J.L. Feugeas. Étude théorique et numérique d'une hiéarchie de modèles aux moments pour le transfert radiatif. C. R. Acad. Sci. Paris, t. 329, SCrie I, p. 915-920, (1999).

[12] R. Duclous, B. Dubroca, and M. Frank. Deterministic Partial Differential Equation Model for Dose Calculation in Electron Radiotherapy. Phys. Med. Biol. 55 3843-3857., 2010.

[13] D. Enskog. Kinetische Theorie der Vorgnge in Mssig Verdnnten Gasen. Uppsala, 1917.

[14] F. Filbet and T. Rey. A hierarchy of hybrid numerical methods for multi-scale kinetic equation. SIAM J. Sci. Computing, 37 Issue: 3 Pages: A1218-A1247 (2015).

[15] González, M., Audit, E., and Huynh, P. Heracles: a three-dimensional radiation hydrodynamics code. *A&A*, 464(2):429–435, 2007.

[16] H. Grad. On the kinetic theory of rarefied gases. Commun. Pure Appl. Math. 2, 331-407 (1949).

[17] E.P. Gross, P.L. Bathnagar, and M. Krook. A Model for Collision Processes in Gases. I. Small Amplitude Processes in Charged and Neutral One-Component Systems. Phys. Rev. 94 (1954), 511.

[18] S. Guisset, D. Aregba, S. Brull, and B. Dubroca. The M1 angular moments model in a velocity-adaptive frame for rarefied gas dynamics applications. Multiscale Model. Simul. 15-4, pp. 1719-1747 (2017).

[19] S. Guisset, S. Brull, B. Dubroca, E. d'Humières, S. Karpov, and I. Potapenko. Asymptotic-preserving scheme for the Fokker-Planck-Landau-Maxwell system in the quasi-neutral regime. Communications in Computational Physics, volume 19, issue 02, pp. 301-328 (2016).

[20] S. Guisset, S. Brull, E. dHumires, B. Dubroca, and V. Tikhonchuk. Classical transport theory for the collisional electronic M1 model. Physica A: Statistical Mechanics and its Applications, Volume 446, Pages 182-194 (2016).

[21] S. Guisset, J.G. Moreau, R. Nuter, S. Brull, E. dHumières, B. Dubroca, and V.T. Tikhonchuk. Limits of the M1 and M2 angular moments models for kinetic plasma physics studies. J. Phys. A: Math. Theor. 48, 335501 (2015).

[22] A. Harten, P.D. Lax, and B. Van Leer. On upstream differencing and Godunov-type schemes for hyperbolic conservation laws. SIAM Review 25 (1983), 35-61.

[23] Philippe Helluy, Michel Massaro, Laurent Navoret, Nhung Pham, and Thomas Strub. Reduced Vlasov-Maxwell modeling. PIERS Proceedings, August 25-28, Guangzhou, 2014, Aug 2014, Gunagzhou, China. pp.2622-2627, 2014.

[24] F. Hermeline. A finite volume method for the approximation of the PN Boltzmann and similar systems of equations on general meshes. CEA Report (2015).

[25] M. Junk and A. Unterreiter. Maximum entropy moment systems and Galilean invariance. Contin. Mech. Thermodyn. 14 (2002), no. 6, 563576.

[26] B. Van Leer. Towards the ultimate conservative difference scheme III. Upstream-centered finite-difference schemes for ideal compressible flow. J. Comput. Phys. 23, 3 (Mar. 1977), 263275.

[27] C.D. Levermore. Moment closure hierarchies for kinetic theories. J. Stat. Phys. 83, 1021-1065 (1996).

[28] J. Mallet, S. Brull, and B. Dubroca. General moment system for plasma physics based on minimum entropy principle. Kinetic and Related Models, vol. 8, No.3, 533-558, (2015).

[29] J. McDonald and M. Torrilhon. An affordable robust moment closures for CFD based on the maximum-entropy hierarchy. J. Comput. Phys. 251, (2013), p. 500-523.

[30] J.G. McDonald and C.P.T. Groth. Towards realizable hyperbolic moment closures for viscous heat-conducting gas flows based on a maximum-entropy distribution. Continuum Mech. Thermodyn. 25, 573-603 (2012).

[31] L. Mieussens. Discrete Velocity Model and Implicit Scheme for the BGK Equation of Rarefied Gas Dynamics. Mathematical Models and Methods in Applied Sciences, 8(10), 1121-1149 (2000).

[32] G.N. Minerbo. Maximum entropy Eddigton Factors. J. Quant. Spectrosc. Radiat. Transfer, 20, 541, (1978).

[33] I. Muller and T. Ruggeri. Rational Extended Thermodynamics. Springer, New York (1998).

[34] G.C. Pomraning. Maximum entropy Eddington factors and flux limited diffusion theory. J. of Quantitative Spectroscopy and Radiative Transfer, 26 5 385-388 (1981).

[35] J.-F. Ripoll. An averaged formulation of the M1 radiation model with presumed probability density function for turbulent flows. J. Quant. Spectrosc. Radiat. Trans. 83 (34), 493517. (2004).

[36] J.-F. Ripoll, B. Dubroca, and E. Audit. A factored operator method for solving coupled radiation-hydrodynamics models. Trans. Theory. Stat. Phys. 31, 531557. (2002).

[37] J. Schneider. Entropic approximation in kinetic theory. ESAIM: M2AN, 38 3 (2004) 541-561.

[38] H. Struchtrup. Macroscopic Transport Equations for Rarefied Gas Flows. Springer, Berlin (2005).

[39] Bingjing Su. More on boundary cpnditions for differential approximations. Journal of Quantitative Spectroscopy and Radiative Transfer 64 (2000) 409-419.

[40] T. Pichard. *PhD thesis*, 2016.

[41] M. Torrilhon. Modeling Nonequilibrium Gas Flow Based on Moment Equations. Annual Review Fluid Mech. 48, (2016), p. 429-458.

[42] R. Turpault. A consistent multigroup model for radiative transfer and its underlying mean opacity. J. Quant. Spectrosc. Radiat. Transfer 94, 357371 (2005).

[43] R. Turpault, M. Frank, B. Dubroca, and A. Klar. Multigroup half space moment appproximations to the radiative heat transfer equations. J. Comput. Phys. 198 363 (2004).